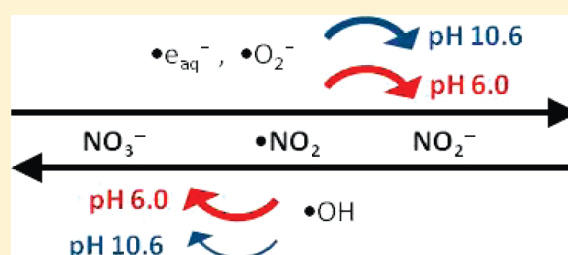


Long-Term γ -Radiolysis Kinetics of NO_3^- and NO_2^- SolutionsPamela A. Yakabuskie,[†] Jiju M. Joseph,[†] Craig R. Stuart,[‡] and J. Clara Wren^{*,†}[†]Department of Chemistry, the University of Western Ontario, London, Ontario, Canada, N6A 5B7[‡]Reactor Chemistry and Corrosion Branch, Atomic Energy of Canada Ltd., Chalk River, Ontario, Canada, K0J 1P0

ABSTRACT: Radiolysis kinetics in NO_3^- and NO_2^- solutions during γ -irradiation were studied at an absorbed dose rate of $2.1 \text{ Gy} \cdot \text{s}^{-1}$ at room temperature. Air- or argon-saturated nitrate or nitrite solutions at pH 6.0 and 10.6 were irradiated, and the aqueous concentrations of molecular water decomposition products, H_2 and H_2O_2 , and the variation in the concentrations of NO_3^- and NO_2^- were measured as a function of irradiation time. The experimental data were compared with computer simulations using a comprehensive radiolysis kinetic model to aid in interpretation of the experimental results. The effect of nitrate and nitrite, present at concentrations below 10^{-3} M , on water radiolysis processes occurs through reactions with the radical species generated by water radiolysis, $\bullet e_{\text{aq}}^-$, $\bullet \text{O}_2^-$, and $\bullet \text{OH}$. The changes in H_2 and H_2O_2 concentrations observed in the presence of nitrate and nitrite under a variety of conditions can be explained by a reduction in the radical concentrations. The kinetic analysis shows that the main loss pathway for H_2 is the reaction with $\bullet \text{OH}$ and the main loss pathways for H_2O_2 are reactions with $\bullet e_{\text{aq}}^-$ and $\bullet \text{OH}$. Nitrate and nitrite compete for the radicals leading to an increase in the concentrations of H_2 and H_2O_2 . Post-irradiation measurements of H_2 , H_2O_2 , NO_2^- and NO_3^- concentrations can be used to calculate the radical concentrations and provide information on the redox conditions of the irradiated aqueous solutions.



1. INTRODUCTION

Many of the current operational and safety issues associated with nuclear power plants are related to materials degradation. Issues include the potential corrosion of the steel piping used in the reactor coolant system or other equipment used to contain radioactive materials. An ability to accurately monitor and control the redox state of the coolant could support strategies to reduce corrosion rates and increase the lifetime of the piping. For example, careful control of the redox conditions of the primary heat transport system during plant outages and start-up to remove oxidants prior to raising the coolant temperature to above $150 \text{ }^\circ\text{C}$ minimizes the risk of degradation of system materials.¹

Associated with corrosion is the formation and transport of dissolved or particulate corrosion products. As the reactor coolant circulates, temperature changes can cause dissolved metal ions and particulates to deposit on system surfaces. Corrosion products transported into the reactor core, or formed in situ in the case of zirconium alloys, can be neutron activated and converted to radioactive isotopes (e.g., ^{54}Mn , ^{58}Co , ^{59}Fe , ^{60}Co , and ^{95}Zr). Recent studies on the radiolysis of slightly acidic aqueous solutions containing dissolved ferrous ions, $\text{Fe}^{2+}(\text{aq})$, have found that uniform-sized colloidal γ - FeOOH particles can be formed.² These colloidal particles can aggregate to form larger particulates. The sizes of the primary particles and the aggregates will depend on the chemical composition and phase structure of the particles and the aqueous redox conditions.³ The production of particulates has important implications for the design of water filtration/purification systems, particle deposition on surfaces, and radioactivity transport in reactor systems.

Optimizing aqueous chemistry in environments where ionizing radiation fields are present requires a detailed understanding of the

chemistry driven by water radiolysis during long duration irradiation. Exposed to ionizing radiation, water decomposes to form a range of chemically reactive species from highly oxidizing ($\bullet \text{OH}$, H_2O_2) to highly reducing ($\bullet e_{\text{aq}}^-$, $\bullet \text{H}$, $\bullet \text{O}_2^-$). The speciation of water radiolysis products changes rapidly (on a microsecond scale) following an initial interaction of the radiation particle (or photon) with the water molecules.⁴ Under continuous irradiation, water decomposition products are continuously produced and these products undergo reactions with each other, with hydrolysis products (such as H^+ and OH^-), and, if present, with solutes and surfaces. Due to fast kinetics of the radical reactions, a system reaches a pseudo-steady state (maintained by the continuous radiation source) on a time scale on the order of milliseconds (note that this is well beyond the submicrosecond time scale typically employed in pulse radiolysis) and then more slowly reaches a true steady state controlled by the presence of slow reactions and interfacial mass transport rates. The steady-state concentrations of the radiolytically produced species determine the aqueous redox conditions that control corrosion or colloid formation from dissolved corrosion products.^{2,5–7}

The steady-state concentrations that develop during continuous γ -irradiation are strongly affected by pH and the presence of dissolved species (even at impurity levels less than 10^{-3} M) if the dissolved species can react readily with water radiolysis products in a pseudocatalytic manner. Due to the many potential oxidation states of N, ranging from -3 in $\text{NH}_3/\text{NH}_4^+$ to $+5$ in NO_3^- under ambient conditions, nitrogen-containing compounds have a

Received: January 10, 2011

Revised: February 28, 2011

Published: April 06, 2011

potential to interact pseudocatalytically with water radiolysis products. For example, NO_3^- can react with reducing species (such as $\cdot e_{\text{aq}}^-$, $\cdot\text{H}$, and $\cdot\text{O}_2^-$) to form NO_2^- and the NO_2^- can then react with oxidizing species (such as $\cdot\text{OH}$ and H_2O_2) to regenerate the NO_3^- . Such a series of reactions can affect the balance of the redox-active species in solution and result in significant changes in their steady-state concentrations.

Nitric acid is used in spent reactor fuel processing and waste treatment, and hydrazine and ammonia are used as pH controlling agents or corrosion inhibitors in nuclear facilities. Degradation of ion exchange resins used for water purification in coolant systems or unintended air ingress may inadvertently introduce nitrogen compounds into the coolant. When such an event occurs, measurement of the nitrogen species present may be used to monitor the coolant redox state.

Our understanding of the radiolysis of nitrate and nitrite in water in a continuous radiation flux is not clear, even after several years of investigation.^{8–12} Better knowledge of the radiation-induced decomposition of nitrate and nitrite is important because this process occurs not only in nuclear systems but also in a wide range of fields such as atmospheric chemistry, UV photolysis, and high-temperature combustion.¹³ In particular, studies of high-flux, continuous radiolysis behavior are very rare. The focus of this work is to identify the set of reactions that control the nitrogen and water radiolysis product speciation during long-term irradiation and to determine how the speciation is affected by the initial solution pH.

2. EXPERIMENTAL SECTION

All solutions were freshly prepared before each experiment with water purified to a resistivity of $18.2 \text{ M}\Omega \cdot \text{cm}$ using a NANOpure Diamond UV ultrapure water system. The experiments at pH 6.0 were performed without the addition of a buffer and those at pH 10.6 used a phosphate buffer (10^{-3} M). The pH of the solution was measured prior to, and at the end of, the irradiation period using a pH meter (Accumet). High-purity sodium nitrate and sodium nitrite were obtained from Sigma-Aldrich (purity $\geq 99\%$) and used without further purification.

Deaerated solutions were prepared by purging the bulk solution with ultra-high-purity argon (Praxair, total impurities $<0.001\%$) for more than one hour. The solution was then transferred into individual 20 mL vials (Agilent Technologies) and sealed, using aluminum crimp caps with PTFE silicone septa, in an argon-filled glovebox where the oxygen level was maintained below 1000 ppm.

The irradiation was carried out in a ^{60}Co gamma cell (MDS Nordion) which provided the irradiation chamber with a uniform absorption dose rate of $2.1 \text{ Gy} \cdot \text{s}^{-1}$ determined using Fricke dosimetry.^{4,14} Individual vials were removed from the irradiation chamber at regular time intervals to perform analysis.

The gaseous H_2 concentration was determined using a gas chromatograph (GC-MS, 6580 Agilent Technologies) equipped with a thermal conductivity detector (TCD), technique detailed in ref 15. With this method, the detection limit for the aqueous H_2 concentration was $1.0 \times 10^{-5} \text{ M}$ and the uncertainties in the measurement arising from sampling and instrumental errors were estimated to be $\pm 50\%$ at the low end of the measured concentration range and $\pm 0.005\%$ at the high end of the concentration range.

All spectrophotometric measurements were performed using a diode array UV spectrophotometer (BioLogic Science Instruments). The concentration of hydrogen peroxide was determined by the Ghormley triiodide method.^{16,17} From a calibration curve, the

Table 1. G Value, Reactions and Rate Constants, and Equilibria Used in the Model Calculations

G Values (Units of Molecules/100 eV)		
reaction no.	formation reaction	G value
R1a	$\text{H}_2\text{O} \rightarrow \cdot e_{\text{aq}}^-$	2.6
R1b	$\text{H}_2\text{O} \rightarrow \text{H}^+$	2.6
R1c	$\text{H}_2\text{O} \rightarrow \text{H}\cdot$	0.6
R1d	$\text{H}_2\text{O} \rightarrow \cdot\text{OH}$	2.7
R1e	$\text{H}_2\text{O} \rightarrow \text{H}_2$	0.45
R1f	$\text{H}_2\text{O} \rightarrow \text{H}_2\text{O}_2$	0.7
Reactions and Rate Constants ($\text{m}^{-1} \cdot \text{s}^{-1}$ or s^{-1})		
	chemical reaction	rate constant (25 °C)
R2	$\cdot e_{\text{aq}}^- + \cdot e_{\text{aq}}^- + 2\text{H}_2\text{O} \rightarrow \text{H}_2 + 2\text{OH}^-$	5.5×10^9
R3	$\cdot e_{\text{aq}}^- + \cdot\text{H} + \text{H}_2\text{O} \rightarrow \text{H}_2 + \text{OH}^-$	2.5×10^{10}
R4	$\cdot e_{\text{aq}}^- + \cdot\text{OH} \rightarrow \text{OH}^-$	3.0×10^{10}
R5	$\cdot e_{\text{aq}}^- + \text{O}_2 \rightarrow \cdot\text{O}_2^-$	2.22×10^{10}
R6	$\cdot e_{\text{aq}}^- + \text{H}_2\text{O}_2 \rightarrow \text{OH}^- + \cdot\text{OH}$	1.6×10^{10}
R7	$\cdot e_{\text{aq}}^- + \text{HO}_2\cdot \rightarrow \text{HO}_2^-$	1.3×10^{10}
R8	$\cdot e_{\text{aq}}^- + \text{HO}_2^- \rightarrow \cdot\text{O}^- + \text{OH}^-$	3.5×10^9
R9	$\cdot e_{\text{aq}}^- + \cdot\text{O}^- + \text{H}_2\text{O} \rightarrow \text{OH}^- + \text{OH}^-$	2.2×10^{10}
R10	$\cdot\text{H} + \cdot\text{OH} \rightarrow \text{H}_2\text{O}$	7×10^9
R11	$\cdot\text{H} + \cdot\text{H} \rightarrow \text{H}_2$	7.75×10^9
R12	$\cdot\text{H} + \text{O}_2 \rightarrow \text{HO}_2\cdot$	2.1×10^{10}
R13	$\cdot\text{H} + \text{HO}_2\cdot \rightarrow \text{H}_2\text{O}_2$	1.0×10^{10}
R14	$\cdot\text{H} + \text{H}_2\text{O}_2 \rightarrow \cdot\text{OH} + \text{H}_2\text{O}$	9.0×10^7
R15	$\cdot\text{H} + \cdot\text{O}_2^- \rightarrow \text{HO}_2^-$	2.0×10^{10}
R16	$\cdot\text{H} + \text{H}_2\text{O} \rightarrow \text{H}_2 + \cdot\text{OH}$	$1.1 \times 10^{11}[\text{H}_2\text{O}]$
R17	$\cdot\text{OH} + \cdot\text{OH} \rightarrow \text{H}_2\text{O}_2$	5.5×10^9
R18	$\cdot\text{OH} + \text{H}_2\text{O}_2 \rightarrow \text{HO}_2\cdot + \text{H}_2\text{O}$	2.7×10^7
R19	$\cdot\text{OH} + \text{H}_2 \rightarrow \text{H}\cdot + \text{H}_2\text{O}$	4.2×10^7
R20	$\cdot\text{OH} + \cdot\text{O}_2^- \rightarrow \text{OH}^- + \text{O}_2^-$	8×10^9
R21	$\cdot\text{OH} + \text{HO}_2\cdot \rightarrow \text{H}_2\text{O} + \text{O}_2$	6×10^9
R22	$\cdot\text{OH} + \text{HO}_2^- \rightarrow \text{HO}_2\cdot + \text{OH}^-$	7.5×10^9
R23	$\cdot\text{OH} + \cdot\text{O}^- \rightarrow \text{HO}_2^-$	2.0×10^{10}
R24	$\cdot\text{O}^- + \text{H}_2\text{O}_2 \rightarrow \cdot\text{O}_2^- + \text{H}_2\text{O}$	2×10^8
R25	$\cdot\text{O}^- + \text{H}_2 \rightarrow \text{H}\cdot + \text{OH}^-$	8.0×10^7
R26	$\cdot\text{O}^- + \text{HO}_2\cdot \rightarrow \cdot\text{O}_2^- + \text{OH}^-$	4.0×10^8
R27	$\cdot\text{O}^- + \text{O}_2 \rightarrow 2\text{OH}^- + \text{O}_2$	6.0×10^8
R28	$\cdot\text{O}^- + \text{O}_2 \rightarrow \cdot\text{O}_3^-$	3.8×10^9
R29	$\cdot\text{O}_3^- \rightarrow \text{O}_2 + \cdot\text{O}^-$	3.0×10^2
R30	$\cdot\text{O}_3^- + \text{H}_2\text{O}_2 \rightarrow \cdot\text{O}_2^- + \text{O}_2 + (\text{H}_2\text{O})$	1.6×10^6
R31	$\cdot\text{O}_3^- + \text{HO}_2\cdot \rightarrow \cdot\text{O}_2^- + \text{O}_2 + \text{OH}^-$	8.9×10^5
R32	$\cdot\text{O}_3^- + \text{H}_2 \rightarrow \text{O}_2 + \text{H}\cdot + \text{OH}^-$	2.5×10^5
R33	$\text{HO}_2\cdot + \cdot\text{O}_2^- \rightarrow \text{HO}_2^- + \text{O}_2$	8.9×10^7
R34	$\text{HO}_2\cdot + \text{HO}_2\cdot \rightarrow \text{H}_2\text{O}_2 + \text{O}_2$	2.0×10^6
R35	$\text{H}_2\text{O}_2 \rightarrow \cdot\text{OH} + \cdot\text{OH}$	2.3×10^{-7}
Related Equilibria and the Equilibrium Rate Constants		
	equilibria	K_{eq}
R36	$\text{H}^+ + \text{OH}^- \rightleftharpoons \text{H}_2\text{O}$	1.78×10^{-16}
R37	$\text{H}^+ + \text{HO}_2^- \rightleftharpoons \text{H}_2\text{O}_2$	1.6×10^{-12}
R38	$\text{H}^+ + \cdot\text{O}_2^- \rightleftharpoons \text{HO}_2\cdot$	1.5×10^{-5}
R39	$\text{H}^+ + \cdot\text{O}^- \rightleftharpoons \cdot\text{OH}$	1.6×10^{-12}
R40	$\text{H}^+ + \cdot e_{\text{aq}}^- \rightleftharpoons \cdot\text{H}$	$k_{40f} = 2.25 \times 10^{10}$ $k_{40b} = 0.63 \times 10^1$

Table 2. Reactions of Nitrate and Nitrite Species with Water Radiolysis Products and Their Rate Constants Used in the Model Calculations

	chemical reaction	rate constant (25 °C)	reference
R41	$\cdot e_{\text{aq}}^- + \text{NO}_3^- \rightarrow \text{NO}_3^{2-}$	9.7×10^9	22
R42	$\text{NO}_3^{2-} + \text{H}_2\text{O} \rightarrow \cdot\text{NO}_2 + 2\text{OH}^-$	5.5×10^4	22, 23
R43	$\cdot e_{\text{aq}}^- + \text{NO}_2^- \rightarrow \text{NO}_2^{2-}$	3.5×10^9	24, 27
R44	$\text{NO}_2^{2-} + \text{H}_2\text{O} \rightarrow \cdot\text{NO} + 2\text{OH}^-$	4.3×10^4	29
R45	$\cdot\text{OH} + \text{NO}_2^- \rightarrow \cdot\text{NO}_2 + \text{OH}^-$	5.0×10^9	27
R46	$\cdot\text{O}_2^- + \text{NO}_3^- \rightarrow \text{NO}_3^{2-} + \text{O}_2$	1.0×10^6	this work ^a
R47	$2\cdot\text{NO}_2 + \text{H}_2\text{O} \rightarrow \text{NO}_3^- + \text{NO}_2^- + 2\text{H}^+$	6.5×10^7	21
R48	$\cdot e_{\text{aq}}^- + \cdot\text{NO}_2 \rightarrow \text{NO}_2^-$	1.0×10^{10}	this work ^b
R49	$\cdot\text{O}_2^- + \cdot\text{NO}_2 \rightarrow \text{NO}_2^- + \text{O}_2$	2.0×10^8	29
R50	$\cdot\text{O}_2^- + \text{NO}_2^- \rightarrow \text{NO}_2^{2-} + \text{O}_2$	5.0×10^6	30
R51	$\cdot\text{OH} + \cdot\text{NO} \rightarrow \text{HNO}_2$	1.0×10^{10}	27
R52	$\cdot\text{O}_2^- + \cdot\text{NO} \rightarrow \text{ONOO}^-$	6.7×10^9	25
R53	$\cdot e_{\text{aq}}^- + \cdot\text{NO} \rightarrow \text{NO}^-$	2.3×10^{10}	26, 27
	equilibria	pK _a	reference
R54	$\text{H}^+ + \text{NO}_3^- \rightarrow \text{HNO}_3$	-1.6	28
R55	$\text{H}^+ + \text{NO}_2^- \rightarrow \text{HNO}_2$	3.4	28
R56	$\text{H}^+ + \text{NO}_3^{2-} \rightarrow \text{HNO}_3^-$	7.5	22
R57	$\text{H}^+ + \text{NO}_2^{2-} \rightarrow \text{HNO}_2^-$	7.7	24
R58	$\text{H}^+ + \text{ONOO}^- \rightarrow \text{ONOOH}$	6.8	28

^a This reaction rate constant was not available in literature and was estimated to be on the order of 10^6 based on other available rate constants for reactions of $\cdot\text{O}_2^-$ with molecular ionic species (e.g., R50). ^b This reaction rate constant was not available in literature and was estimated to be on the order of 10^{10} based on other available rate constants for reactions of $\cdot e_{\text{aq}}^-$ with radical species (e.g., R53).

detection limit for $[\text{H}_2\text{O}_2]$ was determined to be 3×10^{-6} M. The H_2O_2 analysis for samples containing NO_2^- was performed using a reagent where the concentration of the KI was reduced from 0.40 to 0.078 M to minimize any potential interference caused by nitrite species, as described in the literature.¹⁸

The concentration of dissolved nitrite was determined by the Griess method.^{19,20} The sample was first treated with a diazotizing reagent, sulfanilamide, in an acidic medium to form the intermediate diazonium salt. The diazonium salt then reacts with the coupling reagent *N*-(1-naphthyl)-ethylenediamine to form the stable azo compound which has a maximum UV absorption peak at 540 nm with a molar extinction coefficient of $4.0 \times 10^4 \text{ M}^{-1} \cdot \text{cm}^{-1}$.²⁰ Calibration of this analysis method with known nitrite solutions yielded a detection limit for $[\text{NO}_2^-]$ of 3×10^{-6} M.

The concentration of nitrate in the sample solution was determined by reducing the nitrate to nitrite using copper-coated cadmium pellets.^{20,21} The total nitrite concentration formed after reduction ($\text{NO}_3^- + \text{NO}_2^-$) was determined by the above method. The initial nitrate concentration was then calculated as the difference between the nitrite concentration determined following the reduction step reaction and the nitrite concentration determined prior to the reduction step.

3. RADIOLYSIS MODEL

The radiolysis kinetic model used in this study incorporates a comprehensive reaction set for γ -radiolysis of pure water that has been reported previously.¹⁵ This reaction set includes the primary radiolysis production reactions (whose rates are determined by the *G* values multiplied by the radiation dose rate), all of the possible reactions of the radiolysis products with each other (~ 40 elementary homogeneous reactions with well-defined rate constants), hydrolysis reactions, and related acid–base equilibria (see

Table 1). This model has been shown to reproduce the steady-state radiolysis data of liquid water over a wide range of conditions.^{15,22–24}

The effects of dissolved nitrate and nitrite on the steady-state concentrations of radiolysis products have been modeled by incorporating an additional simplified set of reactions of nitrate and nitrite species (13 reactions) with radiolysis products, and associated equilibria (see Table 2). The rate constants for these reactions were taken from the literature.^{25–34} The evolution of these coupled reactions was solved using the software package FACSIMILE. The nitrate/nitrite reaction set included in the model spans nitrogen oxidation states from NO_3^- to NO^- . The reactions of NO^- and further reactions that are associated with forming nitrogen species with an oxidation state lower than +2 are not included in the reaction set. These reactions occur at much longer time scales than the durations of the experimental study and, hence, will not significantly influence the radiolysis kinetics observed in our experiments. Omission of these reactions is supported by our ability to measure a mass balance of stable nitrogen species (nitrate and nitrite) at nearly 100% without including the lower oxidation state nitrogen species.

4. RESULTS

4.1. Experimental Results. The concentrations of the molecular products (H_2 and H_2O_2) of radiolytic decomposition of water and the nitrogen species (NO_3^- and NO_2^-) as a function of irradiation time were measured in aqueous solutions initially containing 10^{-3} M NO_3^- or 10^{-3} M NO_2^- . The results are shown in Figure 1 for pH 6.0/deaerated water and Figure 2 for pH 10.6/deaerated water. For comparison, the results for pure water free of nitrate and nitrite are shown in Figure 3. Also shown in these figures are the results of computer simulations performed using the

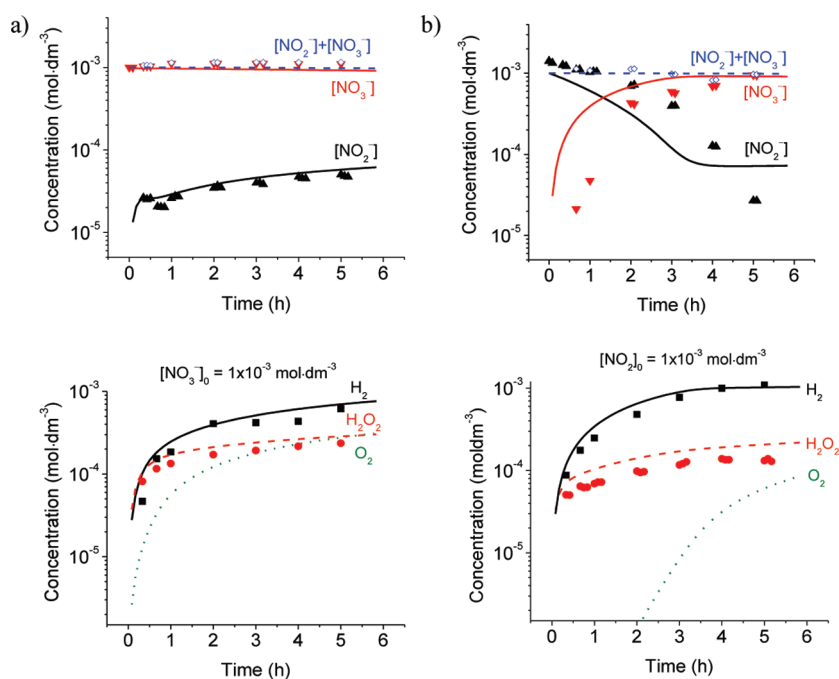


Figure 1. The time-dependent speciation of NO_3^- (red solid triangle down, red solid line) and NO_2^- (black solid triangle up, black solid line), the overall mass balance of nitrogen species (blue open diamond, blue dash line), and the time-dependent concentrations of H_2 (black solid square, black solid line), H_2O_2 (red solid circle, red dash line), and O_2 (green dotted line) at pH 6.0 deaerated condition are shown for aqueous solutions containing (a) $1 \times 10^{-3} \text{ M } [\text{NO}_3^-]_0$ and (b) $1 \times 10^{-3} \text{ M } [\text{NO}_2^-]_0$. Data points represent the experimental data, and the lines are the model simulation results. The total absorbed dose (irradiation time $\times D_R$) for the 5 h irradiation period was 37.8 kGy.

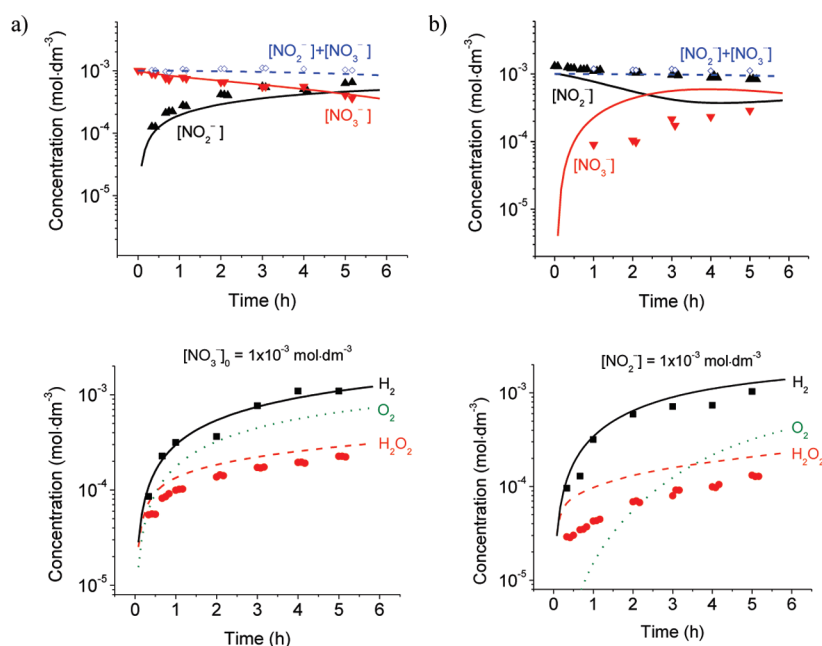


Figure 2. The time-dependent speciation of NO_3^- (red solid triangle down, red solid line) and NO_2^- (black solid triangle up, black solid line), the overall mass balance of nitrogen species (blue open diamond, blue dash line), and the time-dependent concentrations of H_2 (black solid square, black solid line), H_2O_2 (red solid circle, red dash line), and O_2 (green dotted line) at pH 10.6 deaerated condition are shown for aqueous solutions containing (a) $1 \times 10^{-3} \text{ M } [\text{NO}_3^-]_0$ and (b) $1 \times 10^{-3} \text{ M } [\text{NO}_2^-]_0$. Data points represent the experimental data and the lines are the model simulation results. The total absorbed dose (irradiation time $\times D_R$) for the 5 h irradiation period was 37.8 kGy.

radiolysis kinetics model described above. For the pure water case at pH 6.0, the concentrations of H_2O_2 and H_2 were below the detection limit and therefore only the model predictions are shown

in the figure. The pH values of the sample solutions were also measured before and after irradiation. Following the 5 h irradiation period, the change in pH was less than half a pH unit for all samples.

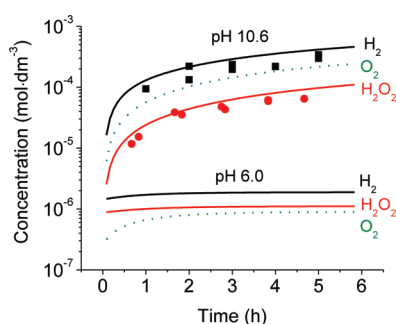


Figure 3. The time-dependent concentrations of H_2 (black solid square, black solid line), H_2O_2 (red solid circle, red dash line), and O_2 (green dotted line) under deaerated condition at pH 6.0 (bottom) and pH 10.6 (top). Data points represent the experimental data and the lines are the model simulation results. At pH 6.0, the measured concentrations of H_2 and H_2O_2 were below the detection limits of 1×10^{-5} and 3×10^{-6} M, respectively. The total absorbed dose (irradiation time $\times D_R$) for the 5 h irradiation period was 37.8 kGy.

For all of the conditions studied, the addition of NO_3^- or NO_2^- increases the radiolytic production of both reducing (H_2) and oxidizing (H_2O_2 and O_2) molecular products, relative to the pure water cases. The addition of nitrate ions increases the H_2O_2 production more than the addition of nitrite ions, while the addition of nitrite increases the H_2 production more than the addition of nitrate. However, the differences between the molecular product concentrations in nitrite and nitrate solutions are small; less than a factor of 2 for all of the tested conditions. In pure water, the concentrations of H_2 and H_2O_2 reached at longer times are a strong function of pH.^{5,15,22} On the other hand, in a solution containing a given nitrogen compound (nitrate or nitrite), the concentrations are nearly independent of pH.

The nitrogen speciation (Figures 1 and 2) shows very different kinetic behavior depending on whether the initial nitrogen species is NO_3^- or NO_2^- . Nevertheless, nitrogen speciation at longer times is nearly independent of the initial nitrogen species but strongly dependent upon pH. An increase in the initial level of dissolved oxygen appears to accelerate the rate of conversion between the nitrate and nitrite (i.e., steady state is reached faster) but has a negligible impact on the resulting steady-state speciation.

4.2. Model Simulation Results. The main objective of the model simulation is to follow the kinetic behavior and concentrations of radical species that are difficult (practically impossible) to monitor directly. The results of model simulations are used in interpreting the overall radiolysis kinetics.

The computer simulation results are in good agreement with the experimental data over a wide range of conditions; the model predictions are within a factor of 2 of the observed data for both the time to reach steady state and the steady-state concentrations. Such agreement is remarkable considering that the radiolysis kinetic model consists of such a large number of different reactions for the radiolysis of pure water plus an additional 13 reactions of water radiolysis products with nitrogen compounds, and we have limited confidence in the rate constants for some of the reactions of nitrogen species. This is particularly true for those slower reactions of nitrogen species with the more “stable” radicals in the system such as $\cdot\text{O}_2^-$. We plan to use the results from this work and future studies to further refine the range of some of those rate constants.

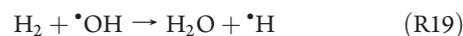
Furthermore, the slight discrepancies between the model-predicted concentrations and the experimentally measured values

(particularly concerning the nitrite fitting results) could be attributed to the assumptions made during the modeling process. First, the model fits were performed on a reduced overall reaction set. The most reduced nitrogen species assumed to form in this model is NO^- . Although a near 100% nitrogen mass balance was measured for most experiments, which validates the use of a simplified reaction set, it is possible that even small contributions from additional reactions involving species of lower nitrogen oxidation state may change the rate of achieving steady state and affect the model fits. Second, the modeling calculations were also performed by holding the pH of the solution constant throughout the irradiation period; hence, the pH was set as a constant parameter. This was deemed to be an appropriate assumption based on the consistency of the experimentally measured pH values (± 0.5 pH unit) before and after irradiation. However, some variations observed between the model simulations and the experimental data may be partially attributed to the ignorance of slight pH changes during the modeling.

5. DISCUSSION

5.1. Radiolysis in the Absence of Nitrate/Nitrite. Previous studies have established the key reactions that determine the concentrations of the molecular water radiolysis products, H_2 and H_2O_2 .^{5,15,22} Among the ~ 40 elementary reactions in Table 1, the key aqueous reactions that control the concentrations of H_2 and H_2O_2 are

For H_2



For H_2O_2



where (R1e) and (R1f) represent the primary homogeneous production by radiolysis and the other reactions are aqueous chemical reactions (reaction numbers are taken from Table 1).

Except at very short time scales (less than milliseconds), the net changes in the concentrations of these species are relatively small. The steady-state approximation can be thus used to obtain analytical solutions for the rate equations. Using only the main reactions listed above, the analytical solutions provide the concentrations for the molecular species as a function of those of the radical species¹⁵

$$[\text{H}_2]_t \approx \frac{k_{\text{rad}}^{\text{H}_2}}{k_{\text{R19}}[\cdot\text{OH}]_t} \quad (\text{E1})$$

$$[\text{H}_2\text{O}_2]_t \approx \frac{k_{\text{rad}}^{\text{H}_2\text{O}_2}}{k_{\text{R6}}[\cdot\text{e}_{\text{aq}}^-]_t + k_{\text{R18}}[\cdot\text{OH}]_t} \quad (\text{E2})$$

where $k_{\text{rad}}^{\text{H}_2} \approx C_R G_{\text{H}_2} D_R \rho_{\text{H}_2\text{O}}$ and $k_{\text{rad}}^{\text{H}_2\text{O}_2} \approx C_R G_{\text{H}_2\text{O}_2} D_R \rho_{\text{H}_2\text{O}}$ represent the zeroth order radiolytic production rates for H_2 and H_2O_2 . These rates are determined by the primary radiolysis yields (the G values), multiplied by the radiation dose rate (D_R) and the density of water ($\rho_{\text{H}_2\text{O}}$) and using a unit conversion

factor (C_R). The other rate constants, k_{R6} , k_{R18} , and k_{R19} , are the second-order rate constants.

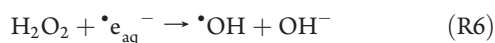
These analytical solutions state that the concentrations of H_2 and H_2O_2 are inversely proportional to the radical concentrations. These inverse relationships were confirmed by the computational results, and good agreement with the data also confirms that the main reactions that control $[H_2]$ and $[H_2O_2]$ are (R1e) and (R19) and (R1f), (R6), and (R18), respectively.¹⁵

For the radical radiolysis products, primary radiolysis (R1) is also the main production pathway but the main removal paths are reactions with molecular species:

For $\bullet OH$



For $\bullet e_{aq}^-$



Note that although (R19) is an important removal path for H_2 , it is not important for the removal of $\bullet OH$ because reactions R18 and R20 are faster. Reaction R19 is only important if H_2 is present at a high concentration prior to the buildup of H_2O_2 and $\bullet O_2^-$.

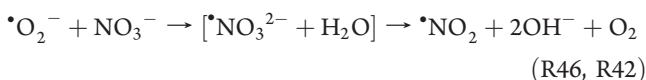
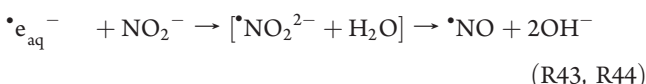
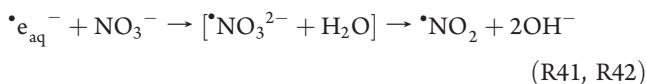
The interaction between the molecular and the radical radiolysis products leads to regeneration of some species that can establish a pseudocatalytic reaction cycle with the radical species. This changes the relative contributions of different reactions to the net removal of the radicals as water radiolysis progresses, making it difficult to predict the net radiolysis production at longer times based on the rates of elementary reactions.^{5,15} For example, for initially deaerated pure water at pH 6.0, the concentrations of the molecular products are below the detection limits and the model simulations also predict values lower than the detection limits as shown in Figure 3. The molecular concentrations remain low at pH 8.5 (results not shown).¹⁵ However, at pH 10.6 the molecular product concentrations are about 3 orders of magnitude larger (Figure 3). These dramatic changes in the molecular product concentrations with pH occur in the pH range 9–11. At pH 10.6, a pH higher than the pK_a of $\bullet H$ of 9.7 ($\bullet H \rightleftharpoons \bullet e_{aq}^- + H^+$), (R40) is very slow and the reaction with secondary radiolysis product, O_2 (reaction R5) becomes an important removal path for $\bullet e_{aq}^-$. The product of (R5), $\bullet O_2^-$, however, reacts with $\bullet OH$ (reaction R20) to re-form O_2 . Once this pseudocatalytic cycle is established, the secondary radiolysis product O_2 can build up to a significant level, while it can continuously react with the radicals. This results in the reduction of the decomposition rates of molecular products, thus, increasing their concentrations (E1 and E2). The significant reduction in the radical concentrations and increase in the molecular concentrations, in pure water at pH 10.6 compared to pH 6.0, are further supported by the computer simulation predictions shown in Figure 4. While a similar cycle can be established between $\bullet H$ and O_2 (leading to $\bullet HO_2$ which can dissociate to H^+ and $\bullet O_2^-$), the H atom cycling will be less effective

than that of the hydrated electron, since the reaction rate constants for the reactions of nitrate and nitrite with $\bullet H$ are approximately 2 orders of magnitude smaller than those with $\bullet e_{aq}^-$. Furthermore, the pseudo-steady-state concentration of $\bullet H$ is not high enough to drive the reactions to comparable rates as those involving $\bullet e_{aq}^-$.¹⁵

Introduction of other chemical species into water that can react with the radical species can upset the chemistry by providing additional removal pathways for those radicals.³⁵ If the added species can be regenerated by back reactions such that they can establish a (semi-) pseudocatalytic cycle with the radical species before they are totally consumed, their influence on radiolysis product concentrations can be significant and last for a long time. Aqueous phase reactions of a chemical additive with the molecular water radiolysis products are typically too slow to be important. However, dissolved additives can affect the molecular product concentrations indirectly, via their interactions with radical species.

5.2. Radiolysis of Aqueous Solutions Initially Containing Nitrate or Nitrite.

5.2.1. Production of H_2 and H_2O_2 . Under all conditions studied, both NO_3^- and NO_2^- increase the radiolytic production of H_2 and H_2O_2 compared to that seen for pure water (Figures 1–3). Dissolved nitrogen species can provide several additional reaction pathways for radical radiolysis products, with the key reactions being



Nitrate and nitrite ion reactions (R41–R45) can compete with (R18) and (R20) for $\bullet OH$ and with (R5), (R6), and R40 for $\bullet e_{aq}^-$ and, at sufficiently high concentrations, can become the dominant removal paths for the radicals. Addition of nitrate/nitrite will lower the net concentrations of $\bullet e_{aq}^-$ and $\bullet OH$, thereby reducing the decomposition rate of H_2 by (R19) and the decomposition rate of H_2O_2 by (R6) and (R18). This can be clearly seen in Figure 4, where the predicted concentrations of $\bullet OH$, $\bullet e_{aq}^-$, and $\bullet O_2^-$ at pH 6.0 and pH 10.6 in solutions with initially dissolved NO_3^- and NO_2^- are compared with those in pure water. At a given pH, the concentrations of all three radicals are substantially lower in the presence of either nitrate or nitrite than those in pure water. The lowered radical concentrations lead to reduced decomposition rates for molecular water radiolysis products and cause the observed increase in the net radiolytic production of H_2 and H_2O_2 in the presence of nitrogen species.

The increases in $[H_2]$ and $[H_2O_2]$ due to the addition of nitrate or nitrite, compared to pure water cases, are larger at pH 6.0 than at pH 10.6. At pH values >9.7, the pK_a of $\bullet H$ ($\bullet H \rightleftharpoons \bullet e_{aq}^- + H^+$), the reaction of $\bullet e_{aq}^-$ with H^+ (R40) is significantly restricted and no longer a main loss path for $\bullet e_{aq}^-$. In pure water, this leads to the establishment of the pseudocatalytic cycle of (R5) and (R20) as described earlier in section 5.1. This substantially increases not only

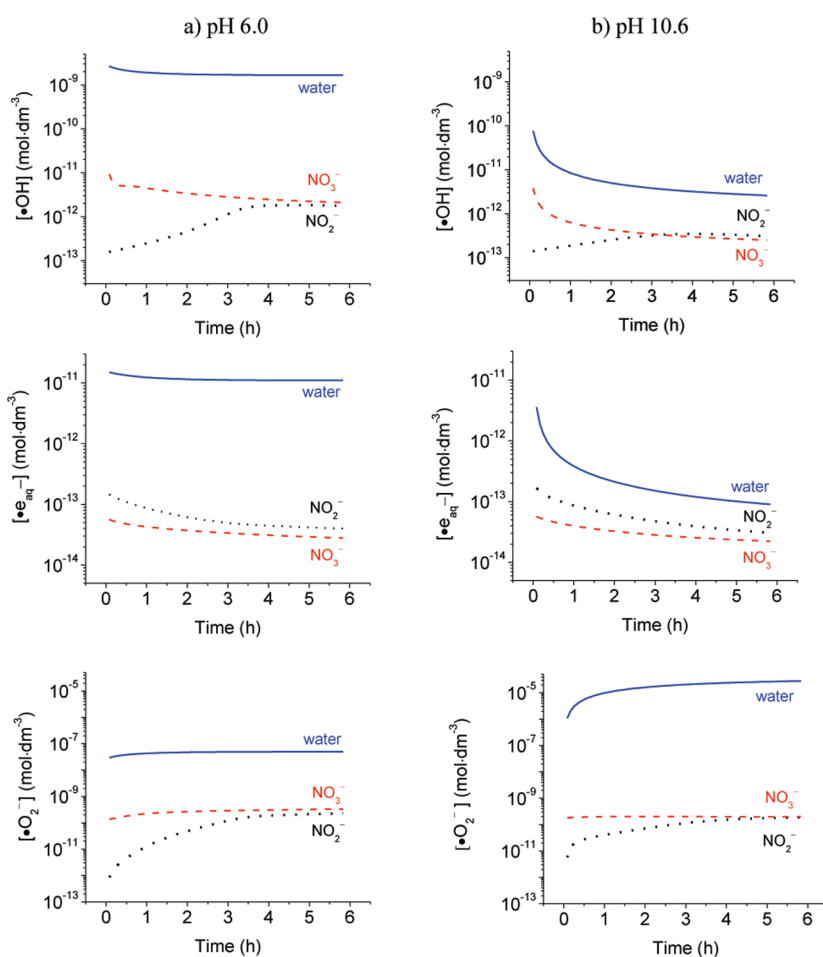


Figure 4. The model simulation results for the time-dependent concentrations of $\bullet\text{OH}$, $\bullet\text{e}_{\text{aq}}^-$, and $\bullet\text{O}_2^-$ achieved in the radiolysis of deaerated solutions of pure water (blue solid line), $[\text{NO}_3^-]_0 = 1 \times 10^{-3} \text{ M}$ (red dash line), and $[\text{NO}_2^-]_0 = 1 \times 10^{-3} \text{ M}$ (black dotted line) at (a) pH 6.0 and (b) pH 10.6. The total absorbed dose (irradiation time $\times D_{\text{R}}$) for the 5 h irradiation period was 37.8 kGy.

$[\text{O}_2]$ but also $[\text{H}_2]$ and $[\text{H}_2\text{O}_2]$ at longer times while decreasing the concentrations of $\bullet\text{OH}$ and $\bullet\text{e}_{\text{aq}}^-$. Nitrate and nitrite will compete for the radicals, mainly with H^+ at pH less than 9.7 (for $\bullet\text{e}_{\text{aq}}^-$, reaction R40), and with the molecular radiolysis products O_2 as well as H_2 and H_2O_2 at pH greater than 9.7 (for $\bullet\text{e}_{\text{aq}}^-$ and $\bullet\text{OH}$, (R5), (R6), and (R18)). Due to significant net radiolysis production of the molecular species at the higher pH, the additional nitrate or nitrite has less influence on the radical concentrations. In pure water, the loss paths for the radicals change as pH changes around the $\text{p}K_{\text{a}}$ of $\bullet\text{H}$. However, in the presence of 10^{-3} M nitrate or nitrite, their main loss paths are the reactions with nitrate and nitrite, and the net water radiolysis production does not vary significantly with pH in the presence of nitrogen-containing species.

At a given pH, the addition of nitrate ions increased H_2O_2 production more than the addition of nitrite ions, while the addition of nitrite increased the H_2 production more than the addition of nitrate. These differences can be partially attributed to the different rate constants of the reactions of NO_3^- and NO_2^- with the radical water radiolysis products, (R41) to (R45). However, the differences in $[\text{H}_2]$ and $[\text{H}_2\text{O}_2]$ are smaller than those expected based on the elementary reaction rate constants. The reaction of NO_3^- with $\bullet\text{e}_{\text{aq}}^-$ has a larger rate constant than the reaction of NO_2^- with $\bullet\text{e}_{\text{aq}}^-$, and a larger increase in $[\text{H}_2\text{O}_2]$ would be expected for radiolysis of nitrate solutions than nitrite solutions.

Similarly, nitrite solutions would be expected to yield a higher $[\text{H}_2]$ than nitrate solutions, since NO_2^- is a good scavenger for $\bullet\text{OH}$, whereas no reaction of $\bullet\text{OH}$ with NO_3^- has been observed.⁸ The computer model indeed predicts initially 2 orders of magnitude higher $[\bullet\text{OH}]$ and a factor of 2 lower $[\bullet\text{e}_{\text{aq}}^-]$ in nitrate solution than those in nitrite solution at both pH values, Figure 4.

The effect of the initial nitrogen species on the net radiolytic production of H_2 and H_2O_2 , however, diminishes with irradiation time, and this can be explained by the radiolytically induced interconversion between nitrate and nitrite. Nitrate and nitrite ions can both participate in a series of redox reactions with reducing (e.g., $\bullet\text{e}_{\text{aq}}^-$, $\bullet\text{O}_2^-$) and oxidizing (e.g., $\bullet\text{OH}$, HO_2^\bullet) species, (R41) to (R46). More importantly, one of their intermediate products, NO_2^\bullet , disproportionates to NO_3^- and NO_2^- at a fast rate. This series of reactions establishes a pseudocatalytic cycle between NO_3^- and NO_2^- . Under continuous irradiation, this will result in a slow net conversion between nitrate and nitrite, while significantly affecting the water radiolysis product concentrations. This explains that even though there is very little net conversion of NO_3^- to NO_2^- the net radiolytic productions of H_2 , H_2O_2 , and O_2 are significant, Figures 1a and 2a.

The competitiveness of nitrate and nitrite for the radicals under a given set of conditions determines the interconversion rate toward a steady state. The concentrations of $\bullet\text{OH}$ and $\bullet\text{O}_2^-$ increase with

time in the nitrite solution while the concentration of $\cdot\text{OH}$ decreases and the concentration of $\cdot\text{O}_2^-$ is nearly constant with time in the nitrate solution. This results in nearly the same steady-state concentrations of the radicals and, hence, the molecular products independent of the initial nitrogen speciation at a given pH. The observed nitrogen speciation at this steady state, where the relative changes in concentrations are small, is thus also nearly independent of whether the initial nitrogen species is NO_3^- or NO_2^- .

5.2.2. *Nitrogen Speciation, $[\text{NO}_3^-]$ and $[\text{NO}_2^-]$.* The pseudocatalytic reactions of the nitrogen compounds with the radicals and their competition with the reactions between radical and molecular water radiolysis products are responsible for the net production of H_2 and H_2O_2 observed under different experimental conditions. Although the nitrogen speciation reached at longer times is nearly independent of the initially dissolved nitrogen species, it is strongly dependent on pH.

Nitrate will initially react with reducing radical species ($\cdot\text{e}_{\text{aq}}^-$ and $\cdot\text{O}_2^-$) to form NO_2^- , but NO_2^- will quickly react with the oxidizing radical species ($\cdot\text{OH}$) to re-form NO_3^- resulting in a slow evolution toward steady-state speciation. Approximate analytical solutions for the concentrations using the steady-state approximation have been developed and compared with the computer predictions. These kinetic analyses have provided an approximate solution for the ratio of NO_2^- and NO_3^-

$$\frac{[\text{NO}_2^-]_t}{[\text{NO}_3^-]_t} \approx \frac{k_{\text{R41}}[\cdot\text{e}_{\text{aq}}^-]_t + k_{\text{R46}}[\cdot\text{O}_2^-]_t}{k_{\text{R45}}[\cdot\text{OH}]_t} \quad (\text{E3})$$

The ratio of NO_2^- to NO_3^- is a function of the concentrations of three radical species, $\cdot\text{e}_{\text{aq}}^-$, $\cdot\text{O}_2^-$, and $\cdot\text{OH}$, and the pH dependence of the ratio arises from the dependence of the radical concentrations on pH. From Figure 4 it is seen that the steady-state concentrations of $\cdot\text{e}_{\text{aq}}^-$ and $\cdot\text{O}_2^-$ do not change when the pH is changed from 6.0 to 10.6. However, the concentration of $\cdot\text{OH}$ is about 10 times lower at pH 10.6 than at pH 6.0, resulting in a change in the ratio of NO_2^- to NO_3^- observed as a function of pH.

The combination of (E1), (E2), and (E3) suggests that the approximate concentrations of the radical species in solution can be determined indirectly from the measurements of H_2 , H_2O_2 , and the steady-state ratio of $[\text{NO}_2^-]$ and $[\text{NO}_3^-]$, providing a complete picture of water radiolysis product distribution. This is a valuable tool for monitoring water chemistry since a combination of the concentrations of the redox active radical species and molecular species determines the aqueous redox potential that controls corrosion behavior.

5.2.3. *Assessment of Nuclear Reactor Data.* The ultimate objective of studying the chemistry of water systems in a radiation field is to be able to predict the chemical behavior and develop effective means to mitigate the damaging consequences of corrosion. We have access to some actual data from operating nuclear power reactors to test our understanding of water radiolysis chemistry. Nitrogen compounds are present in nuclear reactor water systems as a result of either air ingress or deliberate additions of nitrogen-containing compounds. Some CANDU plants experience periodic, inadvertent air ingress into the end shield cooling system. The water in this system (which is maintained at pH 10) is exposed to high fluxes of γ -radiation during reactor operation. Chemistry data for this system at the Point Lepreau Generating Station are shown in Figure 5. The data show that the speciation of nitrogen compounds in the system has more nitrite than nitrate present. This finding is in

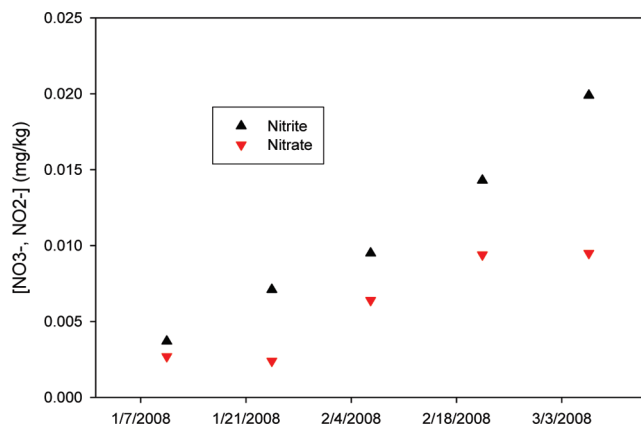


Figure 5. The speciation of NO_3^- (red solid triangle down) and NO_2^- (black solid triangle up), in the end shield cooling system (pH 10) at Point Lepreau Generating Station.

agreement with the results of our work which predict the same trend in speciation, as shown in Figures 1 and 2. The radiolytic production of deuterium (it is a heavy water system), with air ingress, is also elevated in this system, in further agreement with the predictions of our models. We expect that further improvements in our knowledge of the radiation chemistry of nitrogen compounds will support analysis of real reactor chemistry conditions and understanding of the consequences and mitigation of abnormal reactor chemical conditions in the future.

6. CONCLUSIONS

The kinetics of nitrate/nitrite solution radiolysis was followed by monitoring the concentrations of molecular water radiolysis products, H_2 and H_2O_2 , as well as NO_2^- and NO_3^- , as a function of irradiation time. The evolution of the concentrations as a function of irradiation time is described well by reactions of nitrogen species with the radicals generated by the ionizing radiation. The complete reaction kinetics model for radiolysis of nitrate/nitrite solutions was reduced to include only those reactions with highly reducing ($\cdot\text{e}_{\text{aq}}^-$ and $\cdot\text{O}_2^-$) and highly oxidizing ($\cdot\text{OH}$) radicals, and the disproportionation reaction of $\cdot\text{NO}_2$. Analysis using this reduced reaction set demonstrated that it was sufficient to match the observed system chemistry well. Using this reaction set, the ratio of steady-state concentrations of NO_2^- and NO_3^- can be expressed as a simple function of the concentrations of the key water radicals.

This study, which combines experiments and kinetic model analysis, has established a reaction mechanism for the steady-state radiolysis of nitrate and nitrite solutions that can satisfactorily explain data from a nuclear power reactor station as well as laboratory scale experiments. For water systems containing nitrate or nitrite, the concentrations of the redox radical species arising during water radiolysis can be determined from measurements of H_2 , H_2O_2 , and the ratio of NO_2^- and NO_3^- in solution. The ratio of NO_2^- to NO_3^- at steady state is shown to be independent of the initial nitrogen species, but a strong function of pH; at pH values <9.7, the pK_a of $\cdot\text{H}$, nitrate is the dominant species at steady state whereas nitrite is dominant at higher pH values.

AUTHOR INFORMATION

Corresponding Author

*E-mail: jcwren@uwo.ca.

ACKNOWLEDGMENT

The work described herein was funded under the NSERC/AECL (Natural Science and Engineering Research Council of Canada/Atomic Energy of Canada Limited) Industrial Research Chair in Radiation Induced Processes. Support from the Canada Foundation for Innovation New Opportunity grant is greatly acknowledged for the purchase of the Gamma-cell, GC-MSD/TCD, and UV-vis absorption spectrophotometer. The authors thank the NB Power (New Brunswick Power) staff for providing reactor data for the end shield cooling system.

REFERENCES

- (1) Stuart, C. R.; Reid, V.; Turner, C. W. Optimization of Chemistry Control in the Primary Heat Transport System of CANDU Reactors. *Proceedings of the International Conference on Water Chemistry of Nuclear Reactor Systems*, Jeju Island, Korea, Oct 23–26, 2006.
- (2) Yakabuskie, P. A.; Joseph, J. M.; Keech, P.; Botton, G. A.; Guzonas, D.; Wren, J. C. *Phys. Chem. Chem. Phys.* **2011**, *13*, 7198–7206.
- (3) Fu, D.; Keech, P. G.; Sun, X.; Wren, J. C. *Phys. Chem. Chem. Phys.* **2010**, Submitted.
- (4) Spinks, J. W. T.; Woods, R. J. *An Introduction to Radiation Chemistry*; Wiley: New York, 1990.
- (5) Wren, J. C. Steady-state radiolysis: effects of dissolved additives. In *Nuclear Energy and the Environment*; Chien, W., Ed.; ACS Symposium Series, Vol. 1046, American Chemical Society: Washington, DC, 2010; Chapter 22.
- (6) Daub, K.; Zhang, X.; Noël, J. J.; Wren, J. C. *Corros. Sci.* **2011**, *53*, 11–16.
- (7) Daub, K.; Zhang, X.; Noël, J. J.; Wren, J. C. *Electrochim. Acta* **2010**, *55*, 2767–2776.
- (8) Mezyk, S. P.; Bartels, D. M. *J. Phys. Chem. A* **1997**, *101*, 6233–6237.
- (9) Buxton, G. V.; Stuart, C. R. *Chem. J. Soc., Faraday Trans.* **1996**, *92*, 1519–1525.
- (10) Buxton, G. V.; Stuart, C. R. *Chem. J. Soc. Faraday Trans.* **1997**, *93*, 1535–1538.
- (11) Buxton, G. V.; Lynch, D. A.; Stuart, C. R. In *Water Chemistry of Nuclear Reactor Systems 7. Proceedings of the British Nuclear Energy Society Conference*; Bournemouth, United Kingdom, Oct 13–17, 1996; Thomas Telford Publishing: London, 1996; pp 150–152.
- (12) Buxton, G. V.; Lynch, D. A. *J. Chem. Soc., Faraday Trans.* **1998**, *94*, 3271–3274.
- (13) Mezyk, S. P.; Bartels, D. M. *J. Phys. Chem. A* **1997**, *101*, 6233–6237.
- (14) Upadhyay, S. N.; Ray, N. K.; Goel, H. C. *Indian J. Nucl. Med.* **2002**, *17*, 35–41.
- (15) Joseph, J. M.; Choi, B.-S.; Yakabusie, P.; Wren, J. C. *Radiat. Phys. Chem.* **2008**, *77* (9), 1009–1020.
- (16) Hochanadel, C. J. *J. Phys. Chem.* **1952**, *56*, 587–594.
- (17) Stefanic, I.; LaVerne, J. A. *J. Phys. Chem. A* **2002**, *106* (2), 447–452.
- (18) Schwarz, H. A.; Salzman, A. J. *Radiat. Res.* **1958**, *9*, 502–508.
- (19) Slack, P. T. *Analytical Methods Manual*; Leatherhead Food R.A.: London, 1987.
- (20) Sun, J.; Zhang, X.; Broderick, M.; Fein, H. *Sensors* **2003**, *3*, 276–284.
- (21) Cortas, N. K.; Wakid, N. W. *Clin. Chem.* **1990**, *36*, 1440–1443.
- (22) Yakabuskie, P. A.; Joseph, J. M.; Wren, J. C. *Radiat. Phys. Chem.* **2010**, *79*, 777–785.
- (23) Wren, J. C.; Ball, J. M. *Radiat. Phys. Chem.* **2001**, *60*, 577–596.
- (24) Wren, J. C.; Glowa, G. A. *Radiat. Phys. Chem.* **2000**, *58*, 341–356.
- (25) Goldstein, S.; Lind, J.; Merényi, G. *Chem. Rev.* **2005**, *105*, 2457–2470.
- (26) Cook, A. R.; Dimitrijevic, N.; Benjamin, W. *J. Phys. Chem. A* **2001**, *105*, 3658–3666.
- (27) Logager, T.; Sehested, K. *J. Phys. Chem.* **1993**, *97*, 6664–6669.
- (28) Lymar, S. V.; Schwarz, H. A.; Czapski, G. *J. Phys. Chem. A* **2002**, *106*, 7245–7250.
- (29) Goldstein, S.; Czapski, G. *Inorg. Chem.* **1996**, *35*, 5935–5940.
- (30) Seddon, W. A.; Young, M. J. *Can. J. Chem.* **1970**, *48*, 393–394.
- (31) Buxton, G. V.; Greenstock, C. L.; Helman, W. P.; Ross, A. B. *J. Phys. Chem. Ref. Data* **1988**, *17*, 513–886.
- (32) Tretyakov, V. P.; Minko, L. A.; Rudakov, E. S.; Alekhina, T. A. *Theor. Exp. Chem.* **2003**, *39*, 36–40.
- (33) Goldstein, S.; Czapski, G. *Free Radical Biol. Med.* **1995**, *19*, 505–510.
- (34) Bielski, B. H.; Cabelli, D. E.; Arudi, R. L. *J. Phys. Chem. Ref. Data* **1985**, *14*, 1041–1100.
- (35) Allen, A. O.; Hochanadel, C. J.; Ghormley, J. A.; Davis, T. W. *J. Phys. Chem.* **1952**, *56*, 575–586.